International Journal of Heat and Mass Transfer 51 (2008) 5478–5485

Contents lists available at ScienceDirect

International Journal of Heat and Mass Transfer

journal homepage: www.elsevier.com/locate/ijhmt

Evaluation of alternate cooling and heating for tumor treatment

Jianqi Sun, Aili Zhang, Lisa X. Xu *

School of Life Science and Biotechnology, Shanghai Jiao Tong University, Shanghai 200240, PR China

ARTICLE INFO

Article history:
Received 8 November 2007
Received in revised form 4 April 2008
Available online 4 June 2008

Keywords:
Alternate cooling and heating
Tumor treatment
RF heating
Bio-thermal effect

ABSTRACT

A new system aiming for more effective thermal treatment of tumor is presented in this paper. It facilitates liquid nitrogen (LN_2) cooling and radiofrequency (RF) heating in tissue. The bio-heat transfer model has been built to illustrate temperature transients during the treatment, and the induced bio-thermal effects were analyzed at both the tissue and cellular levels. For accurate predictions, the corresponding inactivation energy ΔH of human breast cancer cells (MAD-MB-231) has been obtained through experimental measurements. The results show that through the alternate cooling and heating, the damage region is significantly increased, which cannot be achieved by either the cooling or heating treatment alone.

1. Introduction

Treating tumor with little alteration to the surrounding normal tissue has long been the goal of medical research. In the past two decades, technological advances have brought forth minimally invasive approaches to eliminating undesired tissues. Both cryosurgery and radiofrequency (RF) heating have attracted a great deal of attention.

In cryosurgery, the freezing process causes direct cellular injury, vascular injury, and possible immunologic responses [1]. In addition, it has the benefit of: (1) anesthetic effect of cold; (2) decreased bleeding; (3) and low cost [2]. For cryosurgery of skin cancer, the five-year cure rate has been reported to be 90–98% [3]. However, Rabin and co-workers found that five months after cryosurgery, only about 50% of the tissue in the frozen region was damaged in a sheep breast tumor model [4]. This indicated that for deeply seated tumors, freezing alone might not be enough to completely destroy tumor cells.

On the other hand, RF heating has demonstrated its effectiveness in treating many types of tumors, among the higher temperature treatment methods [5]. Because of the relatively long wavelengths, the RF signals penetrate deeply into the tissue. In the hyperthermia treatment between 43 °C and 45 °C, the tissue temperature mildly raised for a certain period of time is expected to induce cell death by affecting the membrane fluidity, cytoskeletal, protein structure, nuclear structure and disruption of DNA replication [6,7]. But, there are concerns lying in: (1) its effective treatment region, especially in the tumor periphery where the heating is rapidly attenuated by locally augmented blood flow and (2) possible metastasis induced by single local heating [8–10].

To improve tumor shape confirmation during the hyperthermia treatment, researchers have used cool-tip RF probes [11], multi-gauge umbrella RF probes [12], multi-probe arrays [13,14] among others. From the treatment protocol point of view, the idea of combined freezing and heating was first proposed by Gage et al. in 1982. Its effect on increasing the destruction volume was observed experimentally [15]. In 2000, Hoffman et al. performed a histological study of the normal tissue treated by freezing and heating subsequently, and found inconclusive results [8]. Later, Hines-Peralta et al. proposed a hybrid device to enhance the efficiency of a bipolar RF system by placing a freezing unit between the two RF poles [16]. RF heating and cooling based on the Joule–Thomson effect by argon gas were used simultaneously. Their preliminary results showed that with the addition of freezing in the middle of the RF probes, the treated region was enlarged and the shape was better controlled owing to the change of the electrical impedance caused by the ice formation in tissue. Liu et al. also designed a cryo-probe system with vapor heating [17]. They reported that cooling immediately followed by a rapid heating of the target tissue would improve the treatment effect due to thermal stress. However, it is difficult to achieve a rapid heating through conduction only as used in their system, and no biological effect has been demonstrated.

In this study, the effect of alternate cooling and heating on biological tissues has been investigated mechanistically. Using the nude mouse dorsal skin flap chamber tumor model, we have found that tumor cells and vessels were completely destroyed after an alternate treatment, while neither cooling nor heating alone of the same period could induce similar effects [18,19]. In this light, a new thermal system has been designed to provide liquid N_2

* Corresponding author. Tel.: +86 21 34204871; fax: +86 21 34204872.
E-mail address: lisaxu@sjtu.edu.cn (L.X. Xu).

0017-9310/$ - see front matter © 2008 Elsevier Ltd. All rights reserved.
doi:10.1016/j.ijheatmasstransfer.2008.04.027

Nomenclature

A	surface area of cells (m^2)
c	specific heat capacity ($J\ kg^{-1}\ K^{-1}$)
C_t	scale constant in the SAR expression
D	diameter of pipe (mm)
h	convective coefficient ($W\ m^{-2}\ K^{-1}$)
k_s	the inverse of the slope on the exponential portion of the heat inactivation survival curve (s^{-1})
n	the extrapolation number
P	RF power (W)
Pr	Prandtl number
P_k	Planck's constant
q_{met}	volumetric metabolic (J/kg)
r	radial distance (mm)
R	the universal gas constant ($8.314\ J\ mole^{-1}\ K^{-1}$)
r_i	radius of inner tube (mm)
r_o	radius of probe (mm)
Re	Reynolds number
SAR	special absorption rate (W/kg)
S_{cool}	the total cell survival rate during freezing
S_{heat}	the total cell survival rate during heating
T	temperature (K)
T_{seed}	the ice nucleation temperature (K)
T_f	the intracellular phase change temperature (K)
t	thermal treatment in time units (s)
t_{50}	the equivalent time at 50 °C (s)
v	velocity of the nitrogen flow (m/s)
w_b	blood perfusion rate ($ml\ s^{-1}\ ml^{-1}$)
z	axial distance (mm)

Greek symbols

α	a known attenuation constant
γ	Boltzmann's constant
ΔE	the activation energy for the "lethal reaction" (J/mole)
ΔG	the Gibbs free energy of inactivation
ΔH	the inactivation energy (cal/mole)
Δs	the entropy of inactivation in entropy units ($cal\ K^{-1}\ mole^{-1}$)
η	viscosity of the intracellular cytosol ($kg\ m^{-1}\ s^{-1}$)
κ_0	the cell-type dependent constant
λ	thermal conductivity ($W\ m^{-1}\ K^{-1}$)
ξ	the frequency factor constant ($3.1 \times 10^{98}\ s^{-1}$)
ρ	density (kg/m^3)
ω	the rate of thermal injury degree on cellular level
Ω	the rate of thermal injury degree on tissue level
Ω_0	the cell-type dependent constant

Subscripts

a	arterial blood
b	blood
g	gas
i	inner pipe
L	liquid
met	metabolic
t	tissue

cooling and RF heating alternatively. A bio-heat transfer model is built to describe the temperature field during the treatment and to predict the resulted therapeutic effect at the tissue and cellular levels.

2. System design

Fig. 1 shows the new thermal treatment system. For heat transfer enhancement, liquid–gas separator, coiled wire insertions or helical mesh insertions have been considered in the system [20]. It is composed of fourteen units. Liquid nitrogen or nitrogen gas flows out of the Dewar (1), through the liquid–gas separator (7), and into the probe (8). The fluid circulating within the probe generates the freezing effect. The active part of the probe also serves as an RF emission electrode. The probe is made of a metal and the current introduced through the shielded wire (10) inside the probe emitting the RF signals at the active part. A thermocouple is placed inside the probe to monitor the transient temperatures that are collected by the data acquisition system (12) and (14). The measured temperature is compared with the set point to control the electromagnetic valve (6) and the power of an RF generator (13) through a feedback controller. The detailed structure of the cryo-heat probe is illustrated in Fig. 2. It is divided into three segments: the 30 mm long and 2.5 mm diameter active part, the 5 mm diameter vacuum insulation to protect the normal tissue, and the handle. An inner tube (1) of 1 mm diameter is placed inside the probe, through which the nitrogen flows. The flow exits the probe through the outer tube (2) to the exhausting pipe (3). This probe can be cooled to −150 °C in about 2 min, which ensures a rapid cooling as the first step of the treatment. For the subsequent rapid thawing and heating processes, RF has been chosen to achieve deep volumetric heating through longer electric magnetic waves.

3. Heat transfer analysis

The newly designed thermal system enables rapid alternation of cooling and heating in tissue. The system performance has been evaluated through heat transfer modeling. During the thermal treatment, the probe is inserted into the tumor. For simplicity, the tumor can be modeled as a sphere (i.e. 50 mm in radius), and the tip is located at 35 mm from the bottom as illustrated in Fig. 3.

When the liquid–gas separator is set open, vapor and liquid phases in the transportation pipe are stratified due to the difference in densities. The vapor phase, with smaller density, flows above liquid phase, and is ejected through a row of small bores drilled along the upside of the inner pipe. Liquid then flows into the probe. With this separator, the N_2 flow into the probe is set to be in the liquid phase (LN_2) during freezing and in the gas phase during the RF heating. For simulations, the following assumptions are made:

(1) Tissue volume does not change during the treatment, and its density is 970.6 kg/m^3 [21];
(2) The thermal conductivity is constant but at different values in the frozen and unfrozen regions. It changes linearly in the phase transition region [22].

The Pennes equation [23] is used as the governing equation for heat transfer in tissue:

$$\rho_t c_t \frac{\partial T_t}{\partial t} = \nabla(\lambda_t \nabla T_t) + \rho_b c_b w_b (T_a - T_t) + q_{met} + \mathrm{SAR} \quad (1)$$

where t refers to tissue, a arterial blood, b blood, and w_b is the blood perfusion rate ($ml\ s^{-1}\ ml^{-1}$, the volumetric blood flow rate per tissue volume), q_{met} is the volumetric metabolic heat and the specific absorption rate (SAR) of the volumetric RF heating in tissue.

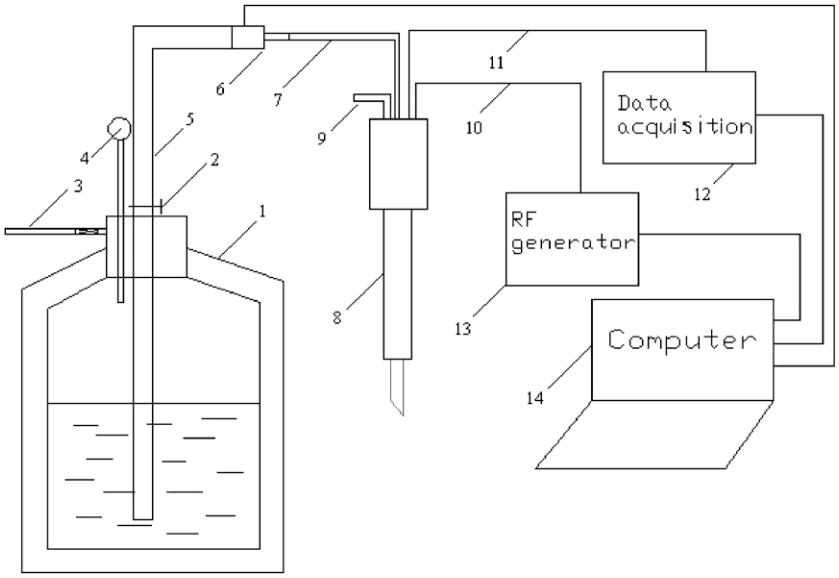

Fig. 1. The newly designed thermal system for breast tumor treatment. 1. Liquid nitrogen Dewar; 2. switch; 3. safety valve; 4. pressure meter; 5. transfer pipe; 6. electromagnetic valve; 7. liquid–gas separator; 8. cryo-heat probe; 9. exhaust pipe; 10. single conductor shielded wire; 11. data-cable; 12. data acquisition system; 13. RF generator; 14. control system.

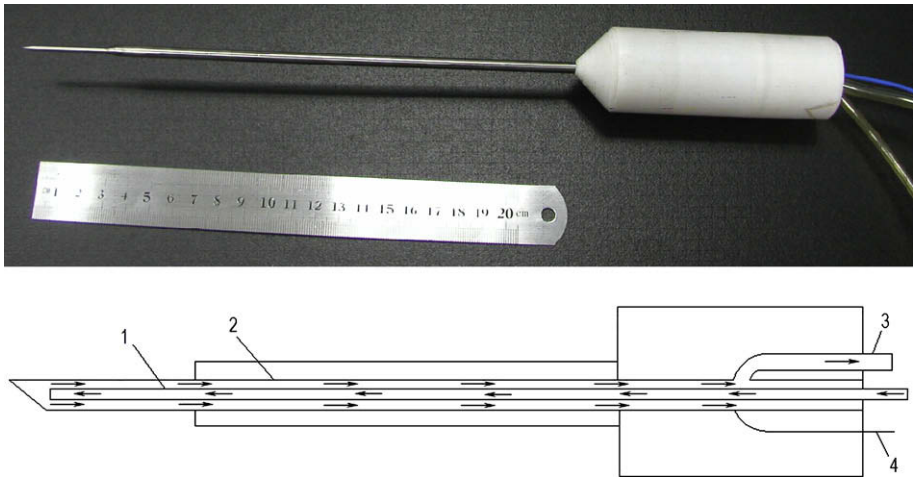

Fig. 2. The cryo-heat probe and its internal structure. 1. Inner tube; 2. outer tube; 3. exhausting pipe; 4. single conductor shielded wire.

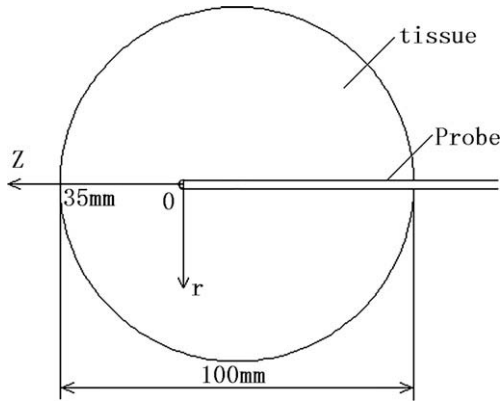

Fig. 3. Physical model of cryo-heat surgery.

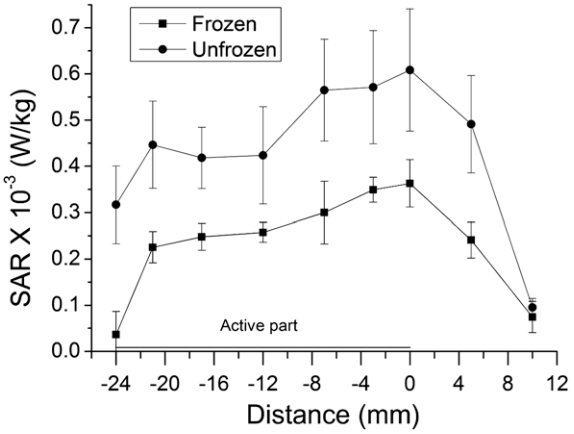

Fig. 4. SAR distributions at 4.5 mm from the probe center in both frozen and unfrozen gels.

In the cylindrical coordinates, the origin locates at the probe tip shown in Fig. 4, the corresponding thermal boundary conditions are:

(1) For the insulated part of the probe:

$$\frac{\partial T_t}{\partial r} = 0 \quad \text{at } r = r_o,\ z \leqslant -30\ \text{mm} \tag{2}$$

where r_o is the probe radius.

(2) For the active part of the probe:

(a) When the inner fluid is in the gas phase, the boundary condition for the tissue contacting the probe surface is

$$\lambda_t \frac{\partial T_t}{\partial r} = h_g(T_t - T_i) \quad \text{at } r = r_o,\ z > -30\ \text{mm} \tag{3}$$

where T_i is the inner-flow temperature and its initial value is the liquid nitrogen temperature −196 °C, h_g is the internal convection coefficient. For the case studied in this paper, a turbulent flow inside the probe is suggested to prevent overheating at the probe surface which would impede the penetration of RF signals in tissue. This probe inner surface can be purposely fabricated to ensure the turbulent flow. The Dittus and Boelter form is used for h_g [24]

$$h_g = 0.023 Re^{0.8} Pr^{0.4} \lambda_L / D \tag{4}$$

where Pr is the Prandtl number, λ_L is the thermal conductivity of nitrogen and D is the probe inner diameter.The flow inside the probe should satisfy the energy conservation law. For a small element of length Δx, one has

$$\rho_g c_g (T_i' - T_i) \cdot \pi (r_o^2 - r_i^2) v = h_g \left(T_t - \frac{T_i + T_i'}{2} \right) \cdot 2\pi r_o \Delta x \quad \text{at } r = r_o,\ 0 > z > -30\ \text{mm} \tag{5}$$

where ρ_g is the nitrogen gas density, c_g is the specific heat, T_i' is the nitrogen bulk temperature on the next node, r_i is the probe inner radius, and v is the flow velocity.

(b) When freezing is turned on, the fluid inside the probe is set to be at −196 °C. The convection effect is considered based on the results reported in [25,26], and the boundary condition for the tissue contacting the probe surface is

$$\lambda_t \frac{\partial T_t}{\partial r} = h_L(T_t - T_i) \quad \text{at } r = r_o,\ z > -30\ \text{mm} \tag{6}$$

where h_l is the empirical convection coefficient for the two-phase flow, approximately 8000 W m^{-2} K^{-1} [25,26].

The thermophysical properties used in the present simulations are taken from literatures [27–29] and listed in Table 1. The apparent specific heat is used to account for the latent heat of tissue solidification [30], where it is represented by two linear functions, which start from 0 °C to −10 °C, respectively, and intersect at −3 °C [31]. It is constant in the frozen and unfrozen regions. According to Song [32], a piecewise linear relationship between blood flow and tissue temperature is assumed during either freezing or heating treatment. Fluent was used to solve Eqs. (1)–(5) and to obtain the temperature distributions inside the tissue during different thermal treatments. A user-defined function (UDF) written in C language is developed to incorporate the boundary conditions and the source terms in the Pennes equation using a similar method developed in [26].

To obtain the volumetric RF heating in tissue, the specific absorption rate (SAR) is measured experimentally. When the RF power is turned on, the surrounding tissue is heated up and tissue temperature rises. The SAR can be calculated from the initial temperature rising rate as the conduction effect is negligible at the beginning of the heating [33]:

$$\text{SAR (W/kg)} = c_p (\partial T / \partial t)|_{t=0^+} \tag{7}$$

where c_p is the specific heat of tissue (J kg^{-1} K^{-1}), T temperature (K) and t time (s). Tissue-equivalent phantom gel is used to electronically mimic tissue at 460 kHz, which is a common frequency used in the commercial RF heating devices. It is prepared according to the formula provided in [34], and the mixture consists of 88.5% water, 5.54% formaldehyde solution (37%), 5.51% gelatin (Sigma Chemical Company, MD), and 0.46% NaCl.

Both the SAR of the frozen and unfrozen gel is measured. In Fig. 4, results show that although the SAR trend in the frozen gel is similar to that in the unfrozen gel, the magnitude is much smaller. This is mainly due to the relatively larger electric resistance caused by the ice formation.

Based on the above measurements, a similar SAR expression is assumed in both frozen and unfrozen tissues but with different scaling factors. By fitting the data to the proposed line source expression [34–36], the SAR expression is obtained:

$$\text{SAR} = \begin{cases} C_t P \frac{(2\alpha r + 1) e^{-2\alpha r}}{r^3}, & -30\ \text{mm} \leqslant z \leqslant 0 \\ 0, & \text{else} \end{cases} \tag{8}$$

where C_t is a scaling constant that is about 670 for unfrozen tissue and 360 for frozen tissue respectively, α (1/m) is a known attenuation constant for the uniform plane wave in a given media and P (W) is the RF power level set during each treatment, and r is the distance from the probe in radius. The heat transfer model is validated with the analytical solutions to the following simplified cases: (1) without blood perfusion and metabolism and (2) constant properties.

Shown in Fig. 5, the dynamic temperature changes have been simulated at different distances from the active probe wall during an alternate cooling and heating treatment. The protocol is 10 min freezing followed by 100 W-RF heating for 30 min with 6.0 m/s nitrogen flow inside the probe. After the 10 min freezing, an iceball is formed, and blood perfusion stops in the area where temperatures are below 0 °C [22].

Also seen in this figure, there is a sharp increase in temperature when the RF heating is turned on. Thermal stresses are expected to occur, and the heterogeneous mechanical properties may lead to more damage inside the tumor than a uniform material experiencing the similar thermal history. Using histopathological analysis, it is found that after the alternate cooling and heating treatment, tumor vessels are completely destroyed, but a cooling or heating treatment for the same period alone could not achieve similar

Table 1
Thermophysical properties of tissue

Thermophysical properties	−10 °C	−3 °C	0 °C	37 °C	42 °C	44 °C	46 °C
Thermal conductivity, k (W/(m K)) [27]	1.56	0.825	0.51	0.51	0.51	0.51	0.51
Specific heat, c_p (kJ/(kg K)) [27]	1.977	47.509[a]	3.689	3.689	3.689	3.689	3.689
Metabolic heat generation, q_{met} (W/m^3) [28,32]	0	0	0	30,000	30,000	30,000	30,000
Blood perfusion rate, w_b (ml s^{-1} ml^{-1}) [27,32]	0	0	0	0.009	0.018	0.036	0

[a] The apparent specific heat formulation is used to account for the phase change of tissue from liquid to solid, a piecewise linear function is assumed with a constraint that the integral of specific heat at phase transit range is equal to the latent heat (250 kJ/kg for tumor tissue), and it peaks at −3 °C according to previous reports [21,31].

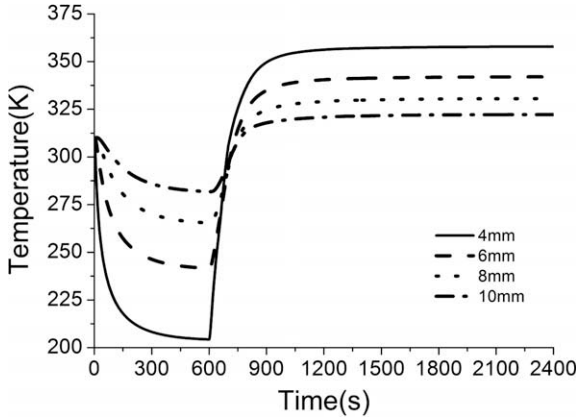

Fig. 5. Dynamic temperature changes at different distances of 4 mm, 6 mm, 8 mm, and 10 mm, respectively, from the active probe wall during an alternate cooling and heating treatment (10 min cooling followed by 100 W-RF heating for 30 min with 6.0 m/s nitrogen flow inside the probe).

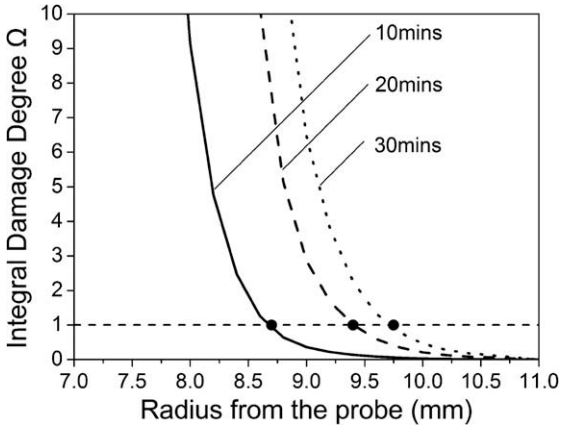

Fig. 6. Damage degree during heating alone for 10, 20 and 30 min, respectively (100 W-RF heating with 6.0 m/s nitrogen flow inside the probe turned on as the probe temperature exceeds 60 °C).

effects [18]. The alternate cooling and heating treatment also enhances damage to the tumor cells. The thermally induced biological effects have been investigated at both the tissue and cellular levels as the follows.

4. Study of bio-thermal damages

4.1. Tissue damage model

The model developed to describe burn injury is frequently applied for evaluation of tissue damage after the heat treatment. The tissue damage process is assumed to follow the Arrhenius function from the thermodynamics point of view [37]. Thus, the rate of injury degree Ω can be described as

$$\frac{d\Omega}{dt} = \xi e^{-\frac{\Delta E}{RT}} \tag{9}$$

It can be integrated as

$$\Omega = \xi \int_0^t e^{-\frac{\Delta E}{RT}} dt \tag{10}$$

where ξ is the frequency factor constant, ΔE is the tissue inactivation energy to govern the development of injury in J/kmole. R is the universal gas constant 8.314 J mole^{-1} K^{-1}, T is the absolute temperature, and t is the thermal treatment in time units.

In clinical applications, values of Ω are usually quantified, and $\Omega = 0.53$, $\Omega = 1.0$, and $\Omega = 10^4$ are associated with the first-degree, second-degree, and third-degree burns, respectively [37,44], which have been defined mainly from the tissue function point of view. In particular, the first-degree burn, which is the least severe, involves only temporary discomfort and a general erythema on the surface. A second-degree burn injury increases the permeability of the vascular endothelium and resulted in the lost of blood perfusion and paler appearance on the skin. The third-degree injury normally causes permanent destruction of the tissue.

Eq. (9) was used to fit to different experimental data sets and different values of the inactivation energy and the scaling constants were obtained by researchers, such as Henriques [38], Fugitt [39], Stoll [40], Takata [41] and Wu [42], and compared by Palla in 1981 [43]. The corresponding Henriques' values of $\xi = 3.1 \times 10^{98}$ s^{-1} and $\Delta E = 6.27 \times 10^8$ J/kmole are used in this study. As proposed by Moritz and Henriques, the second-degree burn $\Omega = 1$ may be evaluated as tissue necrosis [44].

Fig. 6 shows the integral damage degree during heating alone for 10, 20 and 30 min, respectively, as a function of position inside tumor. The vertical axis represents the damage degree, Ω, and the horizontal axis represents the short-axis radius from the probe. The cross point of each curve with the line $\Omega = 1$ has been marked as 8.7 mm, 9.4 mm, and 9.75 mm, respectively. Within these regions where $\Omega > 1$, complete tissue necrosis is assumed.

However, the quantification by Henriques' model only predicts the degree of tissue damage as discussed above. It is difficult to draw the conclusion that all tumor cells have been killed, which is critical in tumor treatment. Any cell survival might result in tumor recurrence or tumor metastasis. Thus, more accurate predictions of the cell survival rate in the treatment region is necessary and of clinical importance.

4.2. Cellular damage model

The life of a cell is sustained by various metabolic activities. Its death may be an accumulation of inactivation of different reactions and denaturation of chromosomal proteins [45], while the damage of each reaction or protein denaturation also follows the Arrhenius function [46–48]:

$$\frac{d\omega}{dt} = k_s = \frac{\gamma T}{P_k} e^{-\Delta G/RT} \tag{11}$$

where ω represents the total damage, k_s is the rate of damage, γ is Boltzmann's constant, P_k is Planck's constant, ΔG is the Gibbs free energy of inactivation which equals $\Delta H - T\Delta s$, where Δs is the entropy of inactivation (cal K^{-1} mole^{-1}), and ΔH is the molecular inactivation energy. An approximate expression for k_s is [47,48]

$$k_s = 2.05 \times (10)^{10} \times T \times e^{\Delta s/2} \times e^{-\Delta H/2T} \tag{12}$$

The occurrence of a complete inactivation of certain reaction and protein denaturation is related to the damage rate k_s and time t. The quantity Δs is an extensive state function that accounts for the effect of irreversibility in a thermodynamic system, and the smallest functional unit in a living system, a cell, can be considered as such a system. As a living cell goes to death, the maximum Δs is expected. In comparison, the differences in Δs between different kinds of live cells and the same cells at different temperatures are relatively small and assume to be negligible. The reported $\Delta s = 374.5$ cal K^{-1} mole^{-1} for CHO cells [45,49] is used in this study.

The fraction of the reactions or the damaged proteins is [48,50,51]

$$F(t) = 1 - e^{-k_s t} \tag{13}$$

Assuming the total cellular damage is an accumulation of n discrete and independent proteins' or reaction inactivations, the survival rate of the cells treated shall follow the equation [46–48]:

$$S_{heat} = 1 - [F(t)]^n = 1 - (1 - e^{-k_s t})^n \tag{14}$$

where S_{heat} is the cell survival rate, and $n = 100$ from [45].

Owing to different sensitivity of cells to heat, the values of inactivation energy ΔH have been reported to be 271,000 cal/mole, 135,600, 141,000, for mouse tumor [52], mouse ear cells [48], and CHO cells[45,49], respectively. As there has been no report of the ΔH value for human breast cancer cell lines, and especially for those exposed to pre-freezing before the heat treatment, experiments have been performed to evaluate the inactivation energy for cells which have undergone different thermal treatments. The mortality of MAD-MB-231 cells heated to different temperatures for different time intervals with or without pre-freezing has been measured by staining of Trypan Blue. By fitting the experimental data to Eq. (14), the inactivation energy ΔH for the cells to heating and heating after pre-freezing to −13 °C for 10 min have been found to be 145,149 cal/mole and 143,898 cal/mole, respectively. The pre-freezing reduces the inactivation energy about 1251 (0.87%) cal/mole compared to direct heating alone, but its effect is significant given the exponential relationship presented by Eq. (14). The results suggest that the cells are more sensitive to heat after the pre-cooling process, and possible synergistic effect has been demonstrated of the alternate cooling and heating treatment.

For further investigation, the cellular survival rate undergone the freezing process is also analyzed. When the cooling rate is slow, extracellular ice forms and water is transported out of the cell causing its osmotic dehydration. The consequent increase of intracellular solute concentrations may induce damage of intracellular proteins, the membrane and enzymatic machinery of the cell. When the cooling rate is fast, there is not enough time for water to be transported out of the cell and intracellular ice forms (IIF) [21,53]. Formation of intracellular ice causes serious damage to the plasma membrane, the organelles and the nucleus membrane also, which are lethal to the cell. For tumor cells closely packed [54], intracellular ice formation shall be the key factor determining the cell death. Thus the survival rate of the tumor cells after freezing can be determined from the intracellular ice formation probability P_{iif}:

$$S_{cool} = 1 - P_{iif} \tag{15}$$

where S_{cool} is the cell survival rate during freezing.

The intracellular ice formation (IIF) probability, P_{iif}, can be predicted given the thermal history that cells experienced [55]:

$$P_{iif} = 1 - \exp\left[-\int_{T_{seed}}^{T} A\Omega_0 \left(\frac{T}{T_{f_0}}\right)\left(\frac{\eta_0}{\eta}\right)\left(\frac{A}{A_0}\right)\exp\left(-\frac{\kappa_0 (T_f/T_{f_0})^4}{\Delta T^2 T^3}\right)\right] \tag{16}$$

where T_{seed} is the ice nucleation temperature (K), Ω_0 and κ_0 are the cell-type dependent constants, A is the surface area, and T_f is the intracellular phase change temperature, which depends on the solute mole fraction, and can be determined by analyzing of the cellular dehydration process [56–59].

Using both the tissue damage model and the cellular damage model, the survival rates of the tumor cells after different treatments are simulated and shown in Fig. 7.

Setting the criterion of $\Omega = 1$ in the tissue damage model, the damage region after the 30 min of RF heating (assuming all tumor cells completely killed within the region) is predicted to be 9.75 mm, shown by the dash-dot line. However, as predicted by the cellular damage model, the region with incomplete cell killing after the RF treatment is clearly illustrated by the dot line in Fig. 7 (8.2 mm in radius). In comparison, the tissue damage model highly overestimates the damaged region by nearly 15%. This model was originally proposed for burn injury evaluation after tissue experiencing a high temperature for a short time period, based on which Abraham and Sparrow had built a more accurate thermal ablation model by accounting for the phase change (water evaporation), the change of blood perfusion and other thermophysical properties [60]. However, it seems not suitable for the hyperthermic condition while tissue temperature is mildly raised over a relatively long period of time.

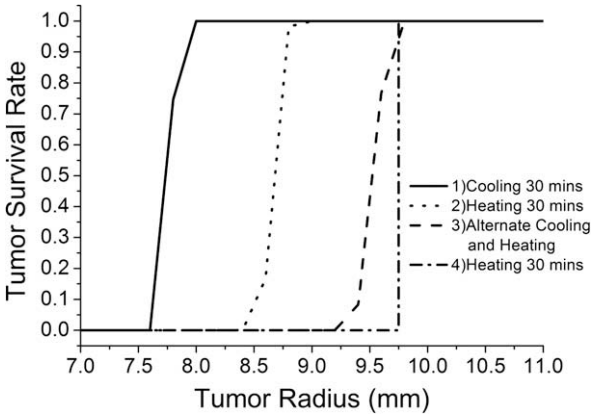

Fig. 7. The survival rate distributions after different protocols: (1) solid line, cooling for 30 min; (2) dotted line, 30 min of the 100 W-RF heating and with 6.0 m/s nitrogen flow inside the probe turned on as the probe temperature exceeds 60 °C; (3) dashed line, 10 min pre-cooling followed by the 100 W-RF heating for 30 min and with 6.0 m/s nitrogen flow inside the probe turned on as the probe temperature exceeds 60 °C; (4) dash-dot line, the tissue damage degree $\Omega = 1$ after 30 min of the 100 W-RF heating and with 6.0 m/s nitrogen flow inside the probe turned on as the probe temperature exceeds 60 °C for 30 min (from Fig. 6).

With the cellular damage model, after cooling alone for 30 min, the complete damage region is only about 7.6 mm in radius from the probe, shown by the solid line. Tumor cells survival rate after the alternate freezing and heating is also determined and shown by the dashed line in Fig. 7. As seen, the influence of a 10 min pre-freezing treatment before the same heating protocol (100 W-RF and with 6.0 m/s nitrogen flow protection turned on as the probe temperature exceeds 60 °C) for 30 min is significant. The complete damage region increases and reaches about 9.2 mm in radius. This is much larger than that caused by either the heating or cooling treatment alone.

5. Conclusions and discussion

In this study, a new thermal system is presented to enhance the efficacy of tumor treatment through a rapid alternation of cooling and heating. The heat transfer analysis and the corresponding cellular damage have been performed to show the system performance. Different models have been used to evaluate the induced damage at both the tissue and cellular levels. Results show that the tissue damage model based on the Arrhenius function cannot be properly used to qualitatively illustrate the degree of tumor damage under the hyperthermic condition. For more accurate predictions, the cellular damage model is suggested to account for the thermo-biological effects.

Comparison of the thermal damage region induced by the alternate cooling and heating treatment to that of either cooling or heating treatment alone clearly demonstrates its advantage. Heat causes cell death through denaturation of proteins and enzymes depending on the thermal dose [45]. The relationship has been quantitatively described using the entropy and the enthalpy of

the inactivation at a given temperature. The cryo-injury to tissue is the result of direct cellular injury and the vascular injury [61]. Direct cellular injury is caused by either extreme dehydration damage to the cellular membranes [62], or intracellular ice formation that tends to disrupt the intracellular organelles and the cell membrane [58,63]. Both of these damages may influence the entropy and enthalpy values. Thus, synergetic therapeutic effects are expected when heat is applied to tissue after it has experienced a pre-freezing process. This is confirmed by fitting the experimental results to the cellular damage model. A decrease of heat inactivation energy is found as the result of pre-freezing, suggesting the increase of cell sensitivity to heat. Given the complex relationship, it is highly desirable to further investigate the underlying mechanisms of such biochemical synergic effects through thermal physical stimulations.

Besides, it is worthy noting that in this study only the direct cellular damage by the alternate cooling and heating has been studied. Given the thermal stress through the rapid alternation of cooling and heating and possible vessel wall fractures induced, the corresponding damage to tumor vasculature is also expected to be greater than that of either the cooling or heating treatment alone, which has already been observed in vivo through our previous experimental study [18]. Moreover, the alternate cooling and heating treatment of tumor may trigger a much stronger immunologic response of the body, which further enhances the overall treatment effect of the system [64]. A comprehensive model should be developed to quantify both the direct and indirect cellular damage for more accurate predictions of the treatment outcome in future.

Acknowledgement

This work has been supported by the National Natural Science Foundation of China (50436030, 50506016) and Shanghai Science and Technology Commission of Shanghai Municipality (05DZ22321).

References

[1] N.E. Hoffmann, J.C. Bischof, The cryobiology of cryosurgical injury, Urology 60 (2A) (2002) 40–49.
[2] R.J. Ablin, An appreciation and realization of the concept of cryoimmunology, in: G.M. Onik, B. Rubinsky, G. Watson, R.J. Ablin (Eds.), Percutaneous Prostate Cryoablation, Quality Medical Publishing Inc., St. Louis, 1995, pp. 136–154.
[3] A.A. Gage, J. Baust, Mechanisms of tissue injury in cryosurgery, Cryobiology 37 (3) (1998) 169–186.
[4] Y. Rabin, T.B. Julian, P. Olson, M.J. Taylor, N. Wolmark, Long-term follow-up post-cryosurgery in a sheep breast model, Cryobiology 39 (1999) 29–46.
[5] A.N. Mirza, B.D. Fornage, N. Sneige, H.M. Kuerer, L.A. Newman, F.C. Ames, S.E. Singletary, Radiofrequency ablation of solid tumors, Cancer J. 7 (2) (2001) 95–102.
[6] D.E. Haines, The pathophysiology of radiofrequency lesion formation, in: D.P. Zipes (Ed.), Catheter Ablation of Arrhythmias, Futura Publishing Co., Inc., Armonk, New York, 1994, pp. 105–127.
[7] R. Hamazoe, M. Maeta, A. Murakami, H. Yamashiro, N. Kaibara, Heating efficiency of radiofrequency capacitive hyperthermia for treatment of deep-seated tumors in the peritoneal cavity, J. Surg. Oncol. 48 (1991) 176–179.
[8] N.E. Hoffmann, B.H. Chao, J.C. Bischof, Cryo, hyper or both? Investigating combination cyro/hyperthermia in the dorsal skin flap chamber, in: Proceedings of the ASME Advances in Heat and Mass Transfer in Biotechnology, 2000, pp. 157–159.
[9] S.A. Shah, Metastasis and hyperthermia. Boca Raton, in: L.J. Anghileri, J. Robert (Eds.), Hyperthermia in Cancer Treatment, CRC Press, Florida, 1986, pp. 191–227.
[10] A. Greenstein, JR. WW. Koontz, Does local hyperthermia affect metastasis of a human prostate carcinoma grown in athymic nude mice, Int. J. Hyperther. 18 (2002) 285–291.
[11] S.N. Goldberg, L. Solbiati, P.F. Hahn, et al., internally cooled electrode technique: laboratory and clinical experience in liver metastases, Radiology 209 (1998) 371–379.
[12] J.F. McGahan, G.D. Dodd III, Radiofrequency ablation of the liver: current status, Am. J. Roentgenol. 176 (1) (2001) 3–16.
[13] S.N. Goldberg, G.S. Gazelle, S.L. Dawson, W.J. Rittman, P.R. Mueller, D.I. Rosenthal, Tissue ablation with radiofrequency using multiprobe arrays, Acad. Radiol. 2 (1995) 670–674.
[14] D. Haemmerich, F.T. Lee Jr., D.J. Schutt, L.A. Sampson, J.G. Webster, D.M. Mahvi, Large volume radiofrequency ablation of ex vivo bovine liver with multiple cooled cluster probes, Radiology 234 (2005) 563–568.
[15] A.M. Gage, M. Montes, A.A. Gage, Destruction of hepatic and splenic tissue by freezing and heating, Cryobiology 19 (1982) 172–179.
[16] A. Hines-Peralta, C.Y. Hollander, S. Solazzo, C. Horkan, Z.J. Liu, S.N. Goldberg, Hybrid radiofrequency and cryoablation device: preliminary results in an animal model, J. Vasc. Intervent. Radiol. 15 (10) (2004) 1111–1120.
[17] J. Liu, Y. Zhou, T. Yu, L. Gui, Z. Deng, Y. Lv, Minimal invasive probe system capable of performing both cryosurgery and hyperthermia treatment on target tumor in deep tissues, Minimal. Invas. Ther. Allied Technol. 13 (1) (2004) 47–57.
[18] Y.Y. Shen, P. Liu, A. Zhang, L.X. Xu, Tumor microvasculature response to alternated cold and heat treatment, in: Proceedings of the Annual International Conference of the IEEE Engineering in Medicine and Biology, 7 vols., 2005, pp. 6797–6800, Art. no. 1616065.
[19] P. Liu, A. Zhang, Y.H. Xu, L.X. Xu, Study of non-uniform nanoparticle liposome extravasation in tumor, Int. J. Hyperther. 21 (3) (2005) 259–270.
[20] S.L. Qi, P. Zhang, R.Z. Wang, A.L. Zhang, L.X. Xu, Development and performance test of a cryoprobe with heat transfer enhancement construction, Cryogenics 46 (2006) 881–887.
[21] A. Zhang, L.X. Xu, G.A. Sandison, J.Y. Zhang, A microscale model for prediction of breast cancer cell damage during cryosurgery, Cryobiology 47 (2003) 143–154.
[22] G. Schuder, G. Pistorius, M. Fehringer, G. Feifel, M.B. Vollma, Complete shutdown of microvascular perfusion upon hepatic cryothermia is critically dependent on local temperature, Br. J. Cancer 82 (4) (2000) 794–799.
[23] H.H. Pennes, Analysis of tissue and arterial blood temperature in resting human forearm, J. Appl. Physiol. (1948) 93–122.
[24] F.W. Dittus, L.M.K. Boelter, Heat transfer in automobile radiators of the tubular type, University of California, Berkeley, Publ. Eng. 2 (13) (1930) 443–461.
[25] A. Zhang, X.D. Luo, C. Chen, L.Q. He, L.X. Xu, Numerical simulation of tissue freezing by liquid nitrogen based cryoprobe, Cryoletters 27 (4) (2006) 243–252.
[26] J.Y. Zhang, G.A. Sandison, J.Y. Murthy, L.X. Xu, Numerical simulation for heat transfer in prostate cancer cryosurgery, J. Biomech. Eng. – Trans. ASME 127 (2) (2005) 279–294.
[27] G.D. Elliott, J.J. McGrath, Freezing response of mammary tissue: a mathematical study, Heat Mass Transfer 44 (1999) 59–64.
[28] J.C. Chato, Thermal properties of tissues, in: R. Skalak, S. Chien (Eds.), Handbook of Bioengineering, McGraw-Hill, New York, 1987 (Chapters 9.1–9.13).
[29] L.X. Xu, L. Zhu, K.R. Holmes, Thermoregulation in the canine prostate during transurethral microwave hyperthermia: Part II. Blood flow response, Int. J. Hyperther. 14 (1) (1998) 65–73.
[30] V.R. Voller, A heat balance integral based on the enthalpy formulation, Int. J. Heat Mass Transfer 30 (1986) 604–606.
[31] Y. Rabin, A. Shitzer, Numerical solution of the multidimensional freezing problem during cryosurgery, J. Biomech. Eng. – Trans. ASME 120 (1998) 32–37.
[32] C.W. Song, Effect of local hyperthermia on blood flow and microenvironment: a review, Cancer Res. 44 (1984) 4721–4730.
[33] T.Z. Wong, J.W. Strohbehn, K.M. Jones, J.A. Mechling, B.S. Trembly, SAR patterns from an interstitial microwave antenna-array hyperthermia system, IEEE Trans. Microwave Theory Tech. 34 (1986) 560–567.
[34] L. Zhu, L.X. Xu, Evaluation of the effectiveness of transurethral radio frequency hyperthermia in the canine prostate: temperature distribution analysis, J. Biomech. Eng. – Trans. ASME 121 (1999) 584–590.
[35] L. Zhu, L.X. Xu, N. Chencinski, The quantification of the 3D electromagnetic power absorption rate produced by the microwave antenna for transurethral prostatic thermotherapy using heat transfer model, AIChE Sympos. Ser. 93 (314) (1997) 168–173.
[36] L. Zhu, L.X. Xu, N. Chencinski, Quantification of the 3D electromagnetic power absorption rate in tissue during transurethral prostatic microwave thermotherapy using heat transfer model, IEEE Trans. Biomed. Eng. 45 (9) (1998) 1163–1172.
[37] K.R. Diller, Modeling of bioheat transfer processes at high and low temperatures, in: Y.I. Cho (Ed.), Bioengineering Heat Transfer, Advances in Heat Transfer, Academic Press, San Diego, 1992, pp. 222–242. 313–357.
[38] F.C. Henriques, Studies of thermal injury. V. The predictability and the significance of thermally induced rate processes leading to irreversible epidermal injury, Arch. Pathol. 43 (1947) 489–502.
[39] C.E. Fugitt, A rate process of thermal injury, Armed Forces Special Weapons Project, AFSWP-606, 1955.
[40] J.A. Weaver, A.M. Stoll, Mathematical model of skin exposed to thermal radiation, National Air Defence Command Memo Report 6708, 1967.
[41] A.N. Takata, Development of criterion for skin burns, Aerospace Med. 45 (1974) 634–637.
[42] Y.C. Wu, A modified criterion for predicting thermal injury, National Bureau of Standards Report, 1980.
[43] R.L. Palla Jr., A heat transfer analysis of scald injury, National Bureau of Standards Report 81-2320, 1981.
[44] A.R. Moritz, F.C. Henriques, Studies of thermal injury. II. The relative importance of time and surface temperature in the causation of cutaneous burns, Am. J. Pathol. 23 (1947) 695–720.

[45] D.C. Dewey, L.E. Hopwood, S.A. Sapareto, L.E. Gerweck, Cellular responses to combinations of hyperthermia and radiation, Radiology 123 (1977) 463–479.
[46] E.L. Carstensen, M.W. Miller, C.A. Linke, Biological effects of ultrasound, J. Biol. Phys. 2 (1974) 173–192.
[47] F.H. Johnson, H. Eyring, M. Palissar, The Kinetic Basis of Molecular Biology, Wiley, New York, 1954. pp. 199, 220, 221, 232, 251, 272, 460.
[48] C.C. Church, Thermal dose and the probability of adverse effects from HIFU, in: C.C. Coussios, G. Haar (Eds.), AIP Conference Proceedings, 2007, pp. 131–137.
[49] A. Westra, W.C. Dewey, Variation in sensitivity to heat shock during the cell-cycle of Chinese hamster cells in vitro, Int. J. Radiat. Biol. 19 (1971) 467–477.
[50] H.A. Johnson, M. Pavelec, Thermal injury due to normal body temperature, Am. J. Pathol. 66 (1972) 557–564.
[51] H.A. Johnson, M. Pavelec, Thermal noise in cells. A cause of spontaneous loss of cell function, Am. J. Pathol. 69 (1972) 119–130.
[52] J. Overgaard, Pathology of heat damage, in: International Symposium on Cancer Therapy by Hyperthermia and Radiation, 1975, pp. 28–30.
[53] P. Mazur, Freezing of living cells: mechanisms and implications, Am. J. Pathol. 143 (1984) C123–C142.
[54] B. Rubinsky, D.E. Pegg, A mathematical model for the freezing process in biological tissue, 234, Proc. Royal Soc. London, Ser. B, Biol. Sci. (1934–1990) 234 (1276) (1988) 343–358.
[55] M. Toner, E.G. Cravalho, M. Karel, Thermodynamics and kinetics of intracellular ice formation during freezing of biological cells, J. Appl. Physiol. 67 (1990) 1582–1593.
[56] R.E. Pitt, Cryobiological implications of different methods of calculating the chemical potential of water in partially frozen suspending media, Cryoletters 11 (1990) 227–240.
[57] J.J. McGrath, Membrane transport properties, in: J.J. McGrath, K.R. Diller (Eds.), Low Temperature Biotechnology: Emerging Applications and Engineering Contributions, BED-vol 10, HTD-vol 98, ASME Press, New York, 1988, pp. 273–330.
[58] R.L. Levin, E.G. Cravalho, C.E. Huggins, A membrane model describing the effect of temperature on the water conductivity of erythrocyte membranes at subzero temperatures, Cryobiology 13 (1976) 415–429.
[59] M.S. Berrada, J.C. Bischof, Evaluation of freezing effects on human microvascular-endothelial cells (HMEC), Cryoletters 22 (2001) 353–366.
[60] J.P. Abraham, E.M. Sparrow, A thermal-ablation bioheat model including liquid-to-vapor phase change, pressure- and necrosis-dependent perfusion, and moisture-dependent properties, Int. J. Heat Mass Transfer 50 (2007) 2537–2544.
[61] D.Y. Gao, J.K. Critser, Mechanisms of cryoinjury in living cells, ILAR J. 41 (4) (2000) 187–196.
[62] J. Wolfe, G. Bryant, Freezing, drying, and/or vitrification of membrane-solute-water systems, Cryobiology 39 (2) (1999) 103–129.
[63] S.K. Balasubramanian, J.C. Bischof, A. Hubel, Water transport and IIF parameters for a connective tissue equivalent, Cryobiology 52 (1) (2006) 62–73.
[64] J.X. Dong, P. Liu, A.L. Zhang, L.X. Xu, Immunologic response induced by alternated cooling and heating of breast cancer, in: Proceedings of 29th IEEE EMBS, 2007.